

Molecular chains and carpets of sexithiophenes on Au(111)

H. Glowatzki,¹ S. Duhm,¹ K.-F. Braun,² J. P. Rabe,¹ and N. Koch^{1,*}

¹Humboldt-Universität zu Berlin, Institut für Physik, Newtonstr. 15, 12489 Berlin, Germany

²Universität Hamburg, Institut für Angewandte Physik, 20355 Hamburg, Germany

(Received 19 February 2007; revised manuscript received 6 June 2007; published 20 September 2007)

The two organic molecular materials α -sexithiophene (6T) and α, ω -dihexylsexithiophene (DH6T) adsorbed on Au(111) in the (sub)monolayer range were investigated by scanning tunneling microscopy (STM) in order to explore the effect of alkyl substitution on the self-assembly at surfaces. Metal substrate step edges are identified as preferred nucleation sites for 6T, while stable nucleus formation for DH6T occurs at kinks of the Au(111) herringbone reconstruction. At low coverage, 6T forms continuous chains of single-molecular width along Au step edges, involving molecular conformation changes by rotations around C-C bonds of neighboring thiophene units. In contrast, DH6T exhibits no ordered structures in the submonolayer range. At monolayer coverage, substantially different structures were observed for the two molecules. 6T forms rows of molecules with parallel long molecular axes, whereas DH6T forms lines along these axes, where the conjugated cores are embedded in a matrix of hexyl chains. Because of different preferred nucleation sites, 6T forms a *continuous* molecular carpet on extended Au(111) terraces, whereas DH6T resembles a *patchworklike* carpet as domain boundaries are induced by the Au(111) herringbone surface structure, leading to reduced domain sizes. Alkylation of 6T thus drastically changes the adsorption behavior and the resulting layer structure on the Au surface. These results should be valuable for developing new directed self-assembly schemes on prepatterned surfaces.

DOI: [10.1103/PhysRevB.76.125425](https://doi.org/10.1103/PhysRevB.76.125425)

PACS number(s): 68.37.Ef, 68.43.-h, 81.07.Nb

I. INTRODUCTION

In recent years, organic molecular semiconductors became recognized as alternative to inorganic materials for the use in (opto)electronic devices (“organic electronics”).^{1–6} Moreover, substantial research efforts are directed towards an ultimate miniaturization of devices—i.e., single- or few-molecular structures exhibiting device functionality—in the context of “molecular electronics.”^{7–12} Both in organic and in molecular electronics, the properties of interfaces formed between functional organic molecules and metals (used, e.g., as electrodes) were identified as key to successful device realization.¹³ Furthermore, spontaneous or directed self-assembly of molecules on surfaces into regular patterns is considered an important feature for bottom-up fabrication processes, since traditional lithography techniques fail on the molecular scale.^{14–19} Therefore, knowledge about the parameters that govern self-assembly on surfaces is decisive for future progress. Key parameters here are the competing interaction strengths between substrate and molecules, on the one hand, and mutual intermolecular interactions, on the other hand. The resulting growth mode, the molecular layer structure, and the electronic properties determine the functionality of devices.

Oligothiophenes are a widely investigated class of conjugated organic molecules for organic and molecular electronics, since materials thereof possess interesting electronic and optical properties—e.g., high charge carrier mobility and absorption and emission in the visible range.^{20–22} In particular, several reports have been published on α -sexithiophene (6T) adsorption on various metal single crystal surfaces—e.g., Ag(110) Ref. 23 and Ag(111) Ref. 24, Cu(110) Ref. 25, Au(110) Ref. 26, and Au(111) Refs. 27 and 28. Rather little is known about an alkyl-substituted analog—i.e., α, ω -dihexylsexithiophene (DH6T).^{22,29–31} A comparative

study of the adsorption of these two molecules, exhibiting an identical conjugated core, on a metal surface should provide information on the influence of alkylation, which should be valuable for future molecular design of directed self-organization schemes. The present scanning tunneling microscopy (STM) experiments show that the addition of two hexyl chains significantly changes several fundamental properties of Au(111) surface-adsorbed layers compared to the nonalkylated parent molecule 6T. Step edges are identified as preferential adsorption sites for 6T, while for DH6T stable nucleus formation occurs at kinks of the Au(111) surface herringbone reconstruction. While pristine 6T forms a layered structure with 6T molecules parallel within a layer reminiscent of bulk crystalline 6T, DH6T forms interdigitated structures where conjugated moieties reside next to alkyl chains. Molecular domain registries relative to the Au substrate were also found to differ for 6T and DH6T. In addition, we observed molecular chains of 6T along Au step edges for submonolayer coverage, where the 6T molecular conformation was significantly changed (compared to both the gas phase and ordered layers on terraces) in order to conform to the metal step-edge shape. Estimations of the energy required for these conformational changes were obtained from density functional theory calculations, providing valuable information on the minimum energy gain by the substrate-molecule interaction upon adsorption.

II. EXPERIMENTAL SETUP

The STM experiments were performed with a VT AFM/STM (Omicron) in a custom ultrahigh-vacuum (UHV) system, comprising interconnected sample preparation (base pressure 1×10^{-9} mbar) and analysis chambers (base pressure 8×10^{-11} mbar). *Ex situ* cut PtIr-tips and etched W tips were used for STM imaging. The Au(111) single crystal

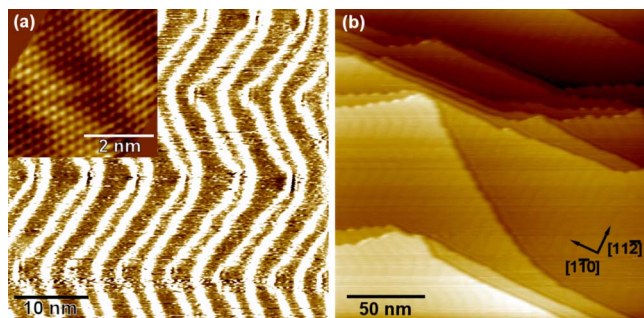


FIG. 1. (Color online) (a) STM image revealing the herringbone reconstruction of the Au(111) surface (-0.09 V, 1.0 nA) and the hexagonal lattice of the surface atoms (inset, -0.03 V, 1.4 nA). (b) Steps and terraces on the Au(111) surface (-0.5 V, 0.5 nA).

(Monocrystals, Inc.) was cleaned by repeated Ar-ion sputtering and annealing (500 °C) cycles. The high quality of the clean Au(111) was confirmed by x-ray photoelectron spectroscopy (no carbon contamination), low-energy electron diffraction (narrow diffraction spots), and STM (clear herringbone surface reconstruction).

6T (Aldrich) and DH6T (H. C. Starck GmbH) were evaporated from homemade resistively heated pinhole sources mounted in the preparation chamber. The deposited mass thickness was monitored with a quartz crystal microbalance, which could be placed at the substrate position. The evaporation rate (ca. 1 Å/min) was thus adjusted prior to each organic molecule deposition onto Au(111). All sample preparation steps and measurements were carried out at room temperature. Unless otherwise noted, the shown STM images are height images.

Molecular orbitals and the energy of various molecular conformations were calculated within the framework of density functional theory (DFT) for the relaxed geometry, however restricted in symmetry for certain conformations. We used the B3LYP functional³² in conjunction with the 6-311G** basis set. Calculations were performed with GAUSSIAN 03.³³

III. RESULTS AND DISCUSSION

A. Clean Au(111) surface

First, we briefly review the Au(111) surface reconstruction, as this will be needed in the further discussion. The Au(111) surface is contracted in the $[\bar{1}10]$ direction compared to the bulk crystal. As a result, the $23 \times \sqrt{3}$ “herringbone” reconstruction forms.³⁴ In STM, the resulting herringbone pattern is clearly visible [Fig. 1(a)]. It is caused by two different surface atom packings, which are separated by small corrugation lines and occur in pairs. Between two closer lines (separation ca. 2.5 nm) hcp packing exists, whereas the wider-distance (separation ca. 3.8 nm) area comprises fcc packing. The lines change their orientation by 120° about every 20 nm. Even if no atomic resolution can be achieved in STM, the herringbone pattern will often be still visible and thus provide information on the surface orientation. The real crystal exhibits relatively large terraces (some-

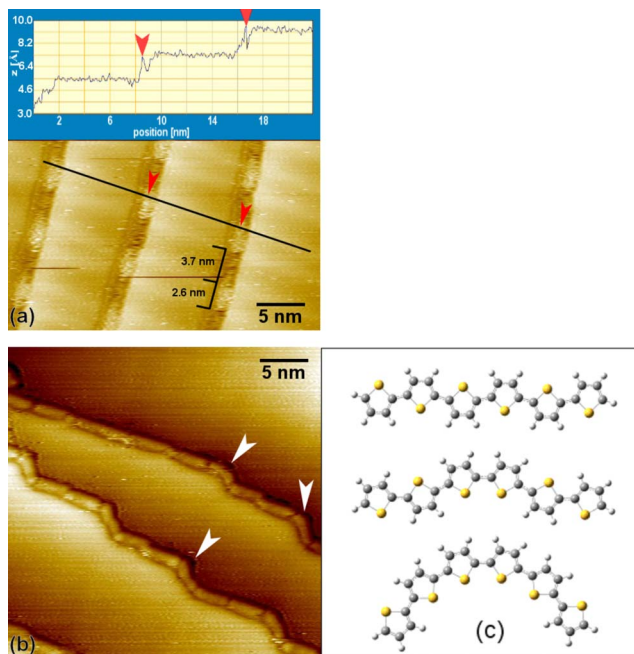


FIG. 2. (Color online) STM images of submonolayer 6T coverage on Au(111). (a) Molecules stick only on hcp positions of the herringbone (-1.5 V, 0.06 nA). Corresponding line profile is shown in the inset. (b) Closed molecular chains (-1.6 V, 0.15 nA) along Au(111) step edges. White arrows mark positions, where the molecules bend around the shape of the step edge. (c) Different 6T geometries used to calculate the energy difference between straight and bent conformations.

times >100 nm wide), separated by one or more atomic steps [c.f. Fig. 1(b)].

B. α -sexithiophene/Au(111)

After depositing a nominal mass thickness of 0.1 nm 6T onto the Au(111) surface we did not observe any ordered molecular clusters or domains on the substrate terraces. Possible reasons for this include that (i) the area density of these ordered domains was very low due to pronounced diffusion and aggregation of 6T molecules on the surface and that (ii) at this low coverage 6T molecules are too mobile to be imaged at room temperature. Note that individual 6T molecules on Au(111) terraces could be observed by STM at substrate temperatures below 10 K.³⁵ However, we found bright features, separated by dark ones, along substrate step edges [Fig. 2(a)], which had an average length of about (2.6 ± 0.2) nm. Since this value is in good agreement with the length of a single 6T molecule, we attribute these features to 6T molecules stabilized at Au step edges. Interestingly, only every second feature along the step edges appeared bright. The average distance between dark features is (3.7 ± 0.2) nm. The position of bright features is clearly correlated with the smaller-distance line periodicity of the Au(111) herringbone pattern—i.e., hcp-packed areas. Consequently, the STM image [Fig. 2(a)] suggests that interrupted 6T molecular chains are formed via self-organization along step edges, addition-

ally modulated by the Au(111) surface reconstruction leading to an occupation of every second available position. From the line profile [inset in Fig. 2(a)] we infer that 6T molecules are residing at the bottom of the edge, which nicely confirms the previously proposed notion that 6T layers on Au(111) terraces start to grow from the bottom of step edges.²⁷ A similar behavior was reported by Chizhov *et al.*³⁶ for Cu-phthalocyanine on Au(111), by Glöckler *et al.*³⁷ for perylene-3,4,9,10-tetracarboxylic-3,4,9,10-dianhydride and N,N'-dimethylperylene-3,4,9,10-bis(dicarboximide) on Ag(111), and by Xiao *et al.*³⁸ for C₆₀ on Au(111), where the molecules formed chains sitting next to step edges, in that last specific case on fcc sites.

At other positions on the sample, we found continuous 6T molecular chains without the bright and dark contrast discussed above [Fig. 2(b)]. Here, molecules are not just sitting on hcp positions, but also on areas with fcc packing. Apparently, all molecules exhibit the same tunneling contrast. An important observation in Fig. 2(b) is that 6T molecules follow the exact shape of the step; i.e., they deviate from their straight conformation in the gas phase and in the bulk. Most likely, bent molecules [some indicated by arrows in Fig. 2(b)] have rotated around the inter-ring C-C bond by 180°. This change in molecular conformation requires energy, which in turn must be gained by the specific interaction around a curved step edge. In order to estimate this energy, we calculated the difference in energy between a 6T molecule in a straight conformation (as optimized in the gas phase), one where the central C-C bond was rotated 180°, and yet another conformation with three inter-ring bonds were rotated [for geometries see Fig. 2(c)]. We found that the energy required per inter-ring bond rotation was smaller than 40 meV in all cases. As this value was obtained by subtracting the energies of two different molecular conformations, we expect negligible errors due to possible underestimations of total molecular energies³⁹ as bond orders for all conformations were conserved. This energy can be regarded as lower limit for the stabilization energy gained by a 6T molecule adopting a bent conformation to follow the Au-step edge. However, since this value is close to the thermal energy at room temperature (ca. 26 meV), the actual stabilization energy may well be larger, since the bent 6T molecules yielded highly stable STM images even at room temperature. In fact, Liu *et al.*⁴⁰ reported that the adsorption energy of a thiophene molecule on a Au(111) defect site, such as a step edge, is ca. 85 meV larger than the adsorption energy on a terrace. This fully supports our observation by STM and the calculated energy required for the 6T conformation changes (<40 meV per inter-ring bond rotation) along step edges. In addition, a non-negligible energy barrier may exist for thiophene units to switch between the two different conformations. In the general context of “molecular wires,” the ability of 6T to adopt the shape of the Au step edge by changes in molecular conformation is remarkable, since most reports on wires made of organic molecules feature mainly straight lines that do not conform to a substrate mediated bent shape.^{41–43}

As the next step, we increased the nominal 6T coverage to 0.2 nm. Apparently, this was sufficient to form a continuous

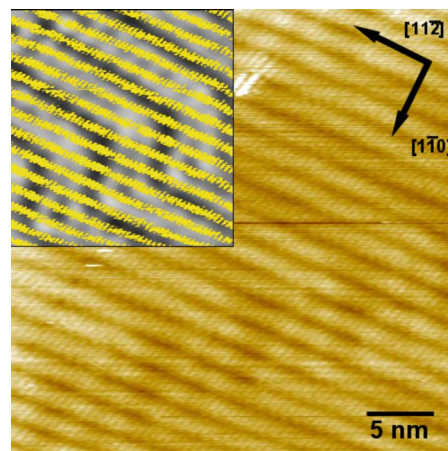


FIG. 3. (Color online) Monolayer of 6T on Au(111), forming a continuous “molecular carpet.” Molecules and herringbone structure are visible simultaneously (−1.4 V, 0.2 nA). The inset shows the same image with enhanced contrast.

layer of 6T, as judged from Fig. 3. Here we can see a highly ordered structure of 6T, arranged in rows. Within a row, the long molecular axes are parallel to each other. We find surface unit cell parameters of $a=(2.3\pm 0.2)$ nm, $b=(0.5\pm 0.1)$ nm, $\alpha=(65\pm 2)^\circ$, and a unit cell area of 1.0 nm². Apparently, the molecules pack rather tight in this structure, as the size of the unit cell already matches the footprint area of a single flat-lying molecule. STM images reveal that the same order persists on very large areas, covering entire Au(111) terraces. Notably, the image shown in Fig. 3 shows contrast due to the 6T monolayer and the Au substrate simultaneously. Since the Au herringbone reconstruction is somewhat difficult to see, we enhanced the contrast by separating the features of the monolayer and substrate in a Fourier analysis (see inset of Fig. 3). There we find an angle between the herringbone reconstruction lines and the long axis of the molecules of about $(37\pm 3)^\circ$. Obviously, the monolayer structure was not influenced by the changes in orientation of the substrate herringbone, as the molecular rows do not follow the direction of the herringbone. Consequently, the interaction between the reconstructed Au surface and the 6T monolayer seems to be rather weak.

Finally, for 6T we observed two different types of submolecular contrast. The first type showed three bright spots [Fig. 4(a)]. The same observation was reported by Mäkinen *et al.*²⁷ for 6T/Au(111) and was explained there by interference effects between the metal surface and the molecules. However, the shape of the tip and the tunneling parameters play an important role in the contrast and therefore the appearance of the molecules in STM experiments. This is exemplified by our second type of submolecular resolution observed for the same sample, where six bright features appear per molecule [Fig. 4(b)], which corresponds to the six individual thiophene units comprising 6T.

C. α,ω -dihexylsexithiophene/Au(111)

At submonolayer coverage of DH6T on Au(111) we were not able to observe any molecule-related structures, neither

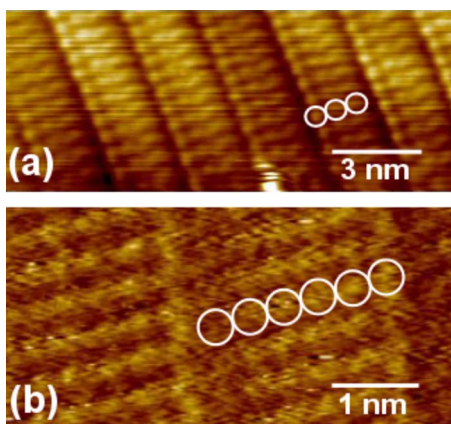


FIG. 4. (Color online) STM image of submolecular resolution of 6T/Au(111) with (a) three inner structures (-1.1 V, 0.6 nA) and (b) six inner structures, corresponding to the six thiophene rings of 6T (current image, -2.0 V, 2.0 nA).

at step edges nor on terraces. This may indicate that Au step edges are not preferred adsorption sites for DH6T. Analogous to the 6T experiments, at about 0.2 nm nominal DH6T coverage on Au(111) complete monolayers were observed (Fig. 5). Depending on the tip and the tunneling conditions, we found bright (high-conductivity) elongated stripes sur-

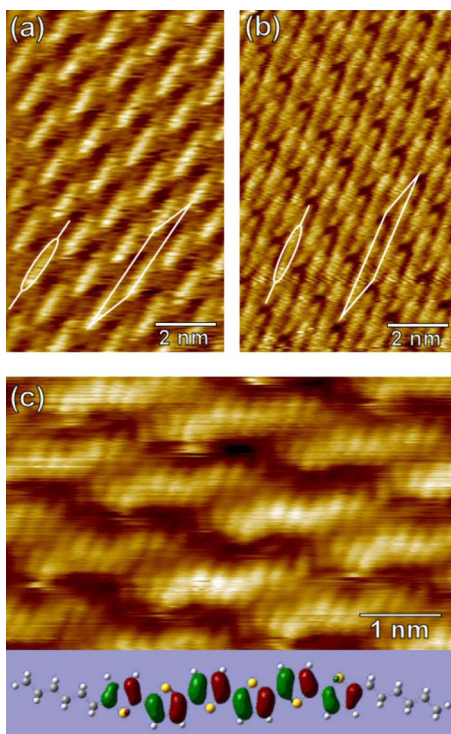


FIG. 5. (Color online) STM image of a monolayer of DH6T on Au(111) at two different imaging contrasts (a) virtually invisible hexyl chains (-0.8 V, 0.5 nA) and (b) clearly visible hexyl chains (-1.0 V, 0.3 nA). A scaled DH6T molecule and the DH6T unit cell are indicated. (c) Submolecular resolution revealing 12 inner structures (-1.1 V, 0.3 nA), corresponding to the DH6T HOMO (bottom).

rounded by comparably dark areas [Fig. 5(a)], as well as rather close packed bright rods (Fig. 5(b)). However, unit cell parameters derived from both images were identical, with $a=(3.7\pm 0.2)$ nm, $b=(1.5\pm 0.1)$ nm, $\alpha=(18\pm 2)^\circ$, and a unit cell area of 1.7 nm². The length of the bright features in Fig. 5(a) (2.2 ± 0.2 nm) corresponds to that of 6T and the length of the bright rods in Fig. 5(b) (3.7 ± 0.2 nm) to that of DH6T. Consequently, we can identify DH6T in both images, while the hexyl chains were not directly distinguishable in Fig. 5(a). Thus the imaging contrast obtained for the hexyl chains is strongly dependent on imaging parameters and the tip. Most notably, the positions of 6T moieties relative to each other for the DH6T monolayer differ significantly from the 6T monolayer/Au(111) (see above). For DH6T, the molecules are not aligned in rows (as for 6T), but assemble in a brick-wall-like structure. Still, molecules are parallel to each other in the direction of the long molecular axes forming lines, but the conjugated cores of neighboring lines are shifted relative to each other along this direction. This leads to very limited side-by-side overlap of thiophene units of neighboring molecules.

The monolayer structure of DH6T/Au(111) is in pronounced contrast to that observed for DH6T on highly oriented pyrolytic graphite (HOPG), which revealed a completely different packing.³¹ There the molecules were also found lying flat on the surface, but in a lamella-like structure, comparable to what we found for 6T/Au(111). Apparently, the DH6T/HOPG interface allows an efficient side-by-side arrangement of the conjugated molecular moieties. Interestingly, maximized phase separation between saturated and conjugated molecular parts was also reported for DH6T assembled in thin films on Si.²² Thus, the metal substrate Au led to an entirely different packing motif, where hexyl and thiophene units exhibit maximized intermixing in two dimensions. This leads to a surface that exposes regularly mixed saturated and unsaturated patches on a molecular level, which may possibly be exploited for future directed self-organization strategies.

Images obtained for DH6T/Au(111) with submolecular resolution reveal 12 bright features within the conjugated 6T core [Fig. 5(c), alkyl chains not visible at these tunneling parameters]. This corresponds to two bright features per thiophene ring, which adequately describes the DH6T highest occupied molecular orbital (HOMO) [bottom of Fig. 5(c)]. The inclination between the molecular-orbital-derived lobes and the long molecular axis in the STM image can be possibly attributed to the convolution of the orbital shape and that of an elongated tip (the tip-sample geometry is fixed in our experiments). Apparently, the bright lobes do not form a straight line, but resemble a wavelike shape. This is expected for 6T cores where thiophene units are in the energetically favorable conformation as shown in the schematic of the DH6T HOMO (i.e., sulfur atoms of neighboring thiophene rings pointing in opposite directions) and thus nicely corroborates our assignment of these features to the DH6T HOMO.

The arrangement of DH6T on Au(111) on a larger scale is shown in Fig. 6(a). Similar to Fig. 3 for 6T, the herringbone is clearly visible in Fig. 6(a) together with DH6T molecules.

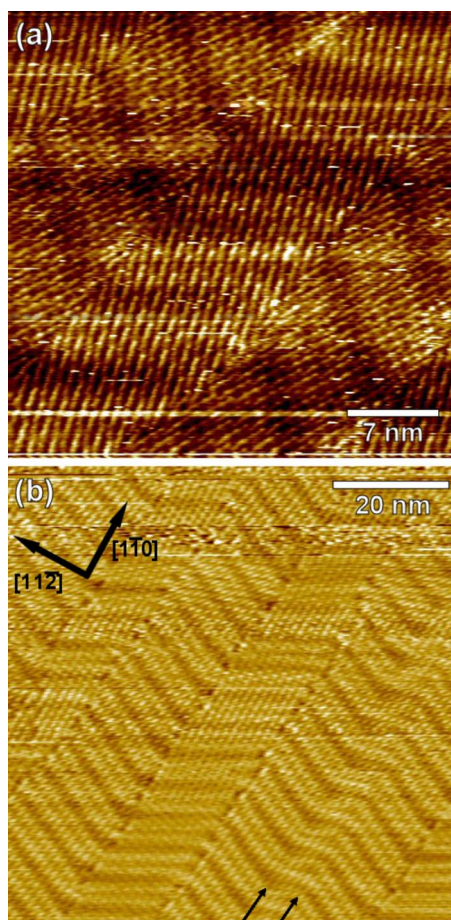


FIG. 6. (Color online) STM images of monolayers of DH6T/Au(111) and herringbone reconstruction. Depending on the herringbone orientation different domains are formed. (a) Different domains are clearly visible (-1.1 V, 0.3 nA). (b) In the lower right corner no new DH6T domain is formed at the short change of the herringbone direction indicated by arrows (-1.1 V, 0.3 nA).

Additionally, several domains are visible, which allows us to infer that the orientation of molecular lines (along their long axis) depends on the orientation of the substrate herringbone pattern. Every kink of the herringbone apparently defines a border of the molecular domain. DH6T molecules exhibit a constant angle of about $(77 \pm 3)^\circ$ relative to the herringbone corrugation lines. Obviously, in the case of DH6T the initial nuclei are formed at the positions of the kink of the herringbone reconstruction. Therefore each orientation of the herringbone reconstruction separately influences the ordering within the molecular domain on top of it, leading to a patchworklike molecular carpet, in contrast to the continuous carpet formed by 6T. An even larger-scale image [Fig. 6(b)] reveals an interesting observation; i.e., no domain boundary in the molecular layer is formed if the domain were to become too small. As shown in a previous work by Tracz *et al.*,⁴⁴ an ordered domain can only exist if the available area is large enough to accommodate the critical nucleus size. As indicated by the arrows in Fig. 6(b), in one case the

distance between two neighboring Au surface reconstruction kinks (and therefore a change of orientation of the herringbone reconstruction) is only ca. 6 nm, whereas typical distances are 15–20 nm. In this specific case, the size of a critical nucleus (typically three to five molecules⁴⁴) could be larger than the distance between the neighboring domains, thus inhibiting the formation of a stable nucleus at this position. Apparently the addition of alkyl chains to the conjugated core prevents nucleation on the step edges as seen for 6T and leads to maximized phase mixing between the separated and conjugated molecular parts.

IV. CONCLUSIONS

We have investigated sexithiophene (6T) and its alkylated analog α,ω -dihexylsexithiophene (DH6T) adsorbed on Au(111) with STM. Evidence is provided that alkyl-chain substitution of a conjugated molecule can have a dramatic impact on a number of fundamental physical properties of adsorbed layers. We found that metal substrate step edges were preferred absorption sites for 6T, resulting in the stable formation of 6T chains of single-molecular width. In order to follow the overall shape of edges, some 6T molecules exhibited bent conformations due to C-C bond rotations between neighboring thiophene units. These initially adsorbed molecules determined the growth direction of domains at higher coverage. Because the monolayer was apparently not affected by changes of the underlying herringbone structure, we conclude that the lateral layer growth is dominated by stable nucleus formation at the Au step edges.

In contrast, for DH6T we observed closed monolayers only, whose domain orientation relative to the substrate was strongly affected by the direction of the Au(111) surface herringbone reconstruction. Corresponding domain boundaries within the organic layer were present at kinks of the Au(111) herringbone reconstruction. Thus, the formation of stable nuclei for DH6T occurred at these kinks of the surface reconstruction, in contrast to the case of 6T. Within the DH6T monolayer, the conjugated molecular parts on neighboring molecules were separated from each other by hexyl chains, leading to a regular nanopattern of conjugated and saturated surface-exposed patches. This surface-induced pattern formation on a molecular scale, which is markedly different from that of the bulk material, may be exploited in future directed self-assembly schemes.

ACKNOWLEDGMENTS

The authors thank Saw-Wai Hla for helpful discussions and H. C. Starck GmbH for kindly providing DH6T. N.K. acknowledges financial support by the Emmy Noether-Program (DFG). Computational Grant No. DMR060005N from the NCSA National Center for Supercomputing Applications and Grant No. PHS0255-1 from the OSC Ohio Supercomputing Center are gratefully acknowledged by K.F.B.

*norbert.koch@physik.hu-berlin.de

- ¹V. Bulovic, G. Gu, P. E. Burrows, S. R. Forrest, and M. E. Thompson, *Nature (London)* **380**, 29 (1996).
- ²S. Möller, C. Perlov, W. Jackson, C. Taussig, and S. R. Forrest, *Nature (London)* **426**, 166 (2003).
- ³J. H. Burroughes, D. D. C. Bradley, A. R. Brown, R. N. Marks, K. Mackey, R. H. Friend, P. L. Burns, and A. B. Holmes, *Nature (London)* **347**, 539 (1990).
- ⁴M. Granstrom, K. Petritsch, A. C. Arias, A. Lux, M. R. Andersson, and R. H. Friend, *Nature (London)* **395**, 257 (1998).
- ⁵B. Crone, A. Dodabalapur, Y. Y. Lin, R. W. Filas, Z. Bao, A. LaDuca, R. Sarpeshkar, H. E. Katz, and W. Li, *Nature (London)* **403**, 521 (2000).
- ⁶M. Pfeiffer, S. R. Forrest, K. Leo, and M. E. Thompson, *Adv. Mater. (Weinheim, Ger.)* **14**, 1633 (2002).
- ⁷Y. Luo, C. P. Collier, J. O. Jeppesen *et al.*, *ChemPhysChem* **3**, 519 (2002).
- ⁸C. Joachim, J. K. Gimzewski, and A. Aviram, *Nature (London)* **408**, 541 (2000).
- ⁹J. M. Tour, L. Jones, D. L. Pearson, J. J. S. Lamba, T. P. Burgin, G. M. Whitesides, D. L. Allara, A. N. Parikh, and S. V. Atre, *J. Am. Chem. Soc.* **117**, 9529 (1995).
- ¹⁰C. A. Mirkin and M. A. Ratner, *Annu. Rev. Phys. Chem.* **43**, 719 (1992).
- ¹¹F. Jäckel, M. D. Watson, K. Müllen, and J. P. Rabe, *Phys. Rev. Lett.* **92**, 188303 (2004).
- ¹²P. Samori, N. Severin, C. D. Simpson, K. Müllen, and J. P. Rabe, *J. Am. Chem. Soc.* **124**, 9454 (2002).
- ¹³*Conjugated Polymer and Molecular Interfaces: Science and Technology for Photonic and Optoelectronic Applications*, edited by W. R. Salaneck, K. Seki, A. Kahn, and J.-J. Pireaux (Marcel Dekker, New York, 2001).
- ¹⁴T. Balgar, S. Franzka, E. Hasselbrink, and N. Hartmann, *Appl. Phys. A: Mater. Sci. Process.* **82**, 15 (2006).
- ¹⁵Y. Lin, A. Boker, J. B. He *et al.*, *Nature (London)* **434**, 55 (2005).
- ¹⁶F. Rosei, M. Schunack, Y. Naitoh, P. Jiang, A. Gourdon, E. Laegsgaard, I. Stensgaard, C. Joachim, and F. Besenbacher, *Prog. Surf. Sci.* **71**, 95 (2003).
- ¹⁷G. P. Lopinski, D. D. M. Wayner, and R. A. Wolkow, *Nature (London)* **406**, 48 (2000).
- ¹⁸L. A. Bumm, J. J. Arnold, L. F. Charles, T. D. Dunbar, D. L. Allara, and P. S. Weiss, *J. Am. Chem. Soc.* **121**, 8017 (1999).
- ¹⁹C. G. Claessens and J. F. Stoddart, *J. Phys. Org. Chem.* **10**, 254 (1997).
- ²⁰L. Torsi, A. Dodabalapur, L. J. Rothberg, A. W. P. Fung, and H. E. Katz, *Science* **272**, 1462 (1996).
- ²¹G. Horowitz, P. Delannoy, H. Bouchriha *et al.*, *Adv. Mater. (Weinheim, Ger.)* **6**, 752 (1994).
- ²²F. Garnier, A. Yassar, R. Hajlaoui, G. Horowitz, F. Deloffre, B. Servet, S. Ries, and P. Alnot, *J. Am. Chem. Soc.* **115**, 8716 (1993).
- ²³H. Inoue, G. Yoshikawa, and K. Saiki, *Jpn. J. Appl. Phys., Part 1* **45**, 1794 (2006).
- ²⁴G. Yoshikawa, M. Kiguchi, S. Ikeda, and K. Saiki, *Surf. Sci.* **559**, 77 (2004).
- ²⁵M. Kiguchi, S. Entani, K. Saiki, and G. Yoshikawa, *Appl. Phys. Lett.* **84**, 3444 (2004).
- ²⁶S. Prato, L. Floreano, D. Cvetko, V. de Renzi, A. Morgante, S. Modesti, F. Biscarini, R. Zamboni, and C. Taliani, *J. Phys. Chem. B* **103**, 7788 (1999).
- ²⁷A. J. Mäkinen, J. P. Long, N. J. Watkins, and Z. H. Kafafi, *J. Phys. Chem. B* **109**, 5790 (2005).
- ²⁸M. Kiel, K. Duncker, C. Hagendorf, and W. Widdra, *Phys. Rev. B* **75**, 195439 (2007).
- ²⁹L. Rossi, G. Lanzani, and F. Garnier, *Phys. Rev. B* **58**, 6684 (1998).
- ³⁰P. Lang, C. Nogues, S. Verneyre, F. Demanze, P. Srivastava, F. Garnier, J. C. Wittmann, B. Lotz, and C. Straupe, *J. Chim. Phys. Phys.-Chim. Biol.* **95**, 1286 (1998).
- ³¹A. Stabel and J. P. Rabe, *Synth. Met.* **67**, 47 (1994).
- ³²A. D. Becke, *J. Chem. Phys.* **98**, 5648 (1993).
- ³³M. J. Frisch *et al.*, in *GAUSSIAN 03*, revision D.1, Wallingford, CT, 2005.
- ³⁴J. V. Barth, H. Brune, G. Ertl, and R. J. Behm, *Phys. Rev. B* **42**, 9307 (1990).
- ³⁵F. Jäckel, V. Iancu, K.-F. Braun, N. Koch, J. P. Rabe, and S.-W. Hla (unpublished).
- ³⁶I. Chizhov, G. Scoles, and A. Kahn, *Langmuir* **16**, 4358 (2000).
- ³⁷K. Glöckler, C. Seidel, A. Soukopp, M. Sokolowski, E. Umbach, M. Böhringer, R. Berndt, and W.-D. Schneider, *Surf. Sci.* **405**, 1 (1998).
- ³⁸W. Xiao, P. Ruffieux, K. Ait-Mansour, O. Gröning, K. Palotas, W. A. Hofer, P. Gröning, and R. Fasel, *J. Phys. Chem. B* **110**, 21394 (2006).
- ³⁹C. E. Check and T. M. Gilbert, *J. Org. Chem.* **70**, 9828 (2005).
- ⁴⁰G. Liu, J. A. Rodriguez, J. Dvorak, J. Hrbek, and T. Jirsak, *Surf. Sci.* **505**, 295 (2002).
- ⁴¹R. Otero, Y. Naitoh, and F. Rosei *et al.*, *Angew. Chem., Int. Ed.* **43**, 2092 (2004).
- ⁴²J. H. Cho, D. H. Oh, and L. Kleinman, *Phys. Rev. B* **65**, 081310(R) (2002).
- ⁴³G. P. Lopinski, D. D. M. Wayner, and R. A. Wolkow, *Nature (London)* **406**, 48 (2000).
- ⁴⁴A. Tracz, A. Stabel, and J. P. Rabe, *Langmuir* **18**, 9319 (2002).